Mechanics Research Communications 128 (2023) 104047

Contents lists available at ScienceDirect

Mechanics Research Communications

journal homepage: www.elsevier.com/locate/mechrescom

Response of 2D and 3D crystal plasticity models subjected to plane strain condition

S. Mirhosseini [a,*], E.S. Perdahcıoğlu [a], E.H. Atzema [a,b], A.H. van den Boogaard [a]

[a] Chair of Nonlinear Solid Mechanics, University of Twente, 7522 NB Enschede, The Netherlands
[b] Tata Steel Research and Development, 1970 CA, IJmuiden, The Netherlands

ARTICLE INFO

Keywords:
Plane strain condition
Computational homogenization
Crystal plasticity
Irregularly shaped RVEs
Periodic boundary conditions

ABSTRACT

The plane strain assumption is generally applied in crystal plasticity finite element (CPFE) simulations in a 2D space to characterize the macroscopic material response considering microstructural features. However, the reliability and accuracy of 2D approximations need to be addressed. In this paper, crystal plasticity finite element simulations of 2D and 3D RVEs are performed with local and averaged plane strain assumptions in Abaqus/Standard. Plane strain postulation is implemented via plane strain elements in 2D and zero average thickness strain in 3D. Irregularly shaped RVEs are generated using the open-source software library Voro++. A conforming mesh is rendered to assign periodic boundary conditions on geometrically periodic RVEs. Periodic boundary condition (PBC) is applied using a prescribed macroscopic deformation gradient tensor. A rate-independent finite strain crystal plasticity model is employed as the user-defined material behavior in finite element simulations. A discrepancy is observed between macroscopic flow curves of 2D and 3D RVEs. The comparison was made for three cases of latent hardening in the crystal plasticity model. In all cases, 3D flow curves exceed 2D results. The results indicate that the deviation is caused by out-of-plane slip activation in 3D simulations, which proves to be an additional hardening source.

1. Introduction

Computational homogenization is an outstanding technique in the multiscale modeling of materials heterogeneities and defects. This method, which is essentially based upon averaging theorems, was first put forth by Babuška [1]. Multiscale methods, in general, bridge various length scales in the materials characterization. The connection between various scales is held through defining an appropriate representative volume element (RVE), first introduced by Hill [2]. The application of RVEs is extended to polycrystalline materials as well. The use of RVEs composed of polycrystalline metals in parallel with the crystal plasticity model as a mesoscale computational technique has absorbed attention in the last decades. This method, defined in a finite element framework, is referred to as crystal plasticity finite element (CPFE) [3].

There is a multitude of studies on material characterization using 3D and 2D CPFE simulations. CPFE analyses are sometimes used in 2D plane stress or plane strain framework for computational efficiency. However, 2D studies fail to predict out-of-plane deformations seen in 3D models [4]. Esmaeilpour et al. [5] highlighted the significance of through-the-thickness shear in single point incremental forming of 7075-O aluminum sheet. In their study, 3D CPFE simulations of the RVEs created from Electron Backscattered Diffraction (EBSD) images were used to calibrate the parameters of the Yld2004-18p yield function. In the study by Vuppala et al. [6], the texture evolution of non-oriented Si-based electrical steels during the rolling process is addressed. The comparison of 3D versus 2D CPFE simulations indicates that 3D simulations can more accurately predict the experimentally measured texture. A microstructure-based RVE approach is used in the study of Ramazani et al. [7] to correlate 2D and 3D flow curves of DP steels. In their study, instead of a crystal plasticity model, a dislocation-based model is used to describe the flow curve of individual phases. It is observed that 2D plane strain underestimates the flow curves of DP steels, while the 3D models result in reasonable predictions compared to the experimental data. Their study claims that the difference between 2D and 3D results is caused by out-of-plane deformation occurring in a 3D model. The observed 2D–3D discrepancy is in agreement with the findings of Thomser [8]. Qayyum et al. [9] investigated the influence of the 3D RVE thickness on stress and strain partitioning in multi-phase materials. The impact of RVE thickness on the global and local stresses and strains is investigated in their study for dual-phase steels. It is concluded that the CPFE simulation of 2D RVEs is suitable for problems in which the global deformation behavior is of interest, whereas a

* Corresponding author.
E-mail address: s.s.mirhosseini@utwente.nl (S. Mirhosseini).

https://doi.org/10.1016/j.mechrescom.2023.104047
Received 11 November 2022; Received in revised form 2 January 2023; Accepted 7 January 2023
Available online 10 January 2023

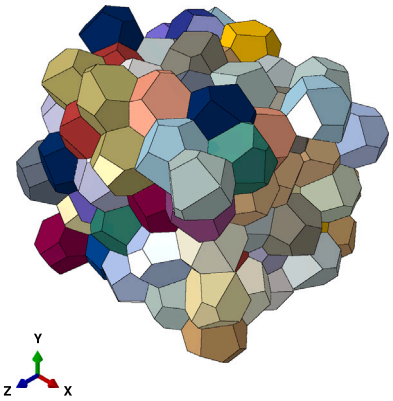

Fig. 1. A 3D irregularly shaped RVE with 125 grains.

3D RVE is necessary to determine stabilized and more accurate local deformation behavior. Knezevic et al. [10] used 2D and 3D CPFE simulations of polycrystalline microstructures to capture 3D topological effects on the microstructural evolution during the rolling process. This study indicates that 3D effects are clearly missing in 2D planar CPFE simulation results and highlights the significance of 3D simulations.

The influence of local plane strain assumption in 2D space is investigated in the current work. This planar assumption is generally used in CPFE simulations to predict mechanical material response. Consequently, local and averaged plane strain conditions are adopted in crystal plasticity finite element simulations of 2D and 3D arbitrarily shaped RVEs, respectively. This goal is achieved by plane strain elements in a 2D model and a zero average thickness strain in a 3D one. Once volume elements are generated using the Voro++ software library, a conforming mesh is rendered to simplify the assignment of periodic boundary conditions. The attribution of PBC is performed through the prescription of a macroscopic deformation gradient tensor. As the material model, a rate-independent finite strain crystal plasticity model is utilized at each Gauss point. Once the size of the 2D and 3D RVEs is determined, finite element simulations are performed to capture the macroscopic stress–strain curves.

The paper has the following outline: Section 2 gives a summary of the crystal plasticity model. Section 3 briefly explains the approach used in computational homogenization. Section 4 elaborates on the numerical results, including the discrepancy between 2D and 3D flow curves.

2. Crystal plasticity model

Crystal plasticity is a powerful computational method to capture diverse micromechanical phenomena. There is a multitude of studies on the crystal plasticity modeling of the material constitutive behavior. Acharya [11] developed a continuum theory of the elastic–plastic response of a single crystal using the theory of continuously distributed dislocations. In the investigation by Forest et al. [12], the Cosserat crystal plasticity model is applied to handle size effects observed in metals. Bammann [13] developed a crystal plasticity model embedded with a natural length scale within the framework of Coleman–Gurtin thermodynamics of internal state variables. Mayeur and McDowell [14] proposed a rate-dependent three-dimensional crystal plasticity model for duplex Ti–6Al–4V alloy that accounts for the distinct 3D slip geometry for both phases, length scale-dependent and anisotropic slip strengths, non-planar prismatic dislocation core structure, and crystallographic texture.

A rate-independent finite strain crystal plasticity model [15] is employed as the material model at each integration point in the finite element simulations in Abaqus/Standard. Rate-independent formulation avoids adding any artificial numerical rate sensitivity and contributes to addressing the discrepancy of the macroscopic material response exposed to local plane strain condition in 2D and averaged plane strain condition in 3D concisely. In this model, crystallographic slip on each slip system is assumed as the mere mechanism for plastic deformation; the deformations caused by twinning and transformation-induced plasticity are ignored. For further details of the model, the reader is referred to the study of Asaro [16] and Clayton [17].

Each slip system α is represented by a unit vector in the slip direction $\mathbf{s}_0^{(\alpha)}$ and slip plane normal $\mathbf{n}_0^{(\alpha)}$ defined in the reference configuration. Deformation is postulated to occur in two stages: a plastic deformation from a reference configuration to an intermediate configuration followed by an elastic rotation from the intermediate configuration to the final configuration. The total velocity gradient $\mathbf{L} = \mathbf{D}+\mathbf{W}$ (in which $\mathbf{D}$ is the rate of deformation and $\mathbf{W}$ is spin tensor) is decomposed in an elastic part $\mathbf{L}_e$ and a plastic part $\mathbf{L}_p$.

$$\mathbf{L} = \mathbf{L}_e + \mathbf{L}_p \tag{1}$$

The plastic part of the total velocity gradient tensor is defined as the summation over all slip systems of the shear rates $\dot{\gamma}^{(\alpha)}$ multiplied by the Schmid tensor computed as $\mathbf{P}^{(\alpha)} = \mathbf{s}^{(\alpha)} \otimes \mathbf{n}^{(\alpha)}$;

$$\mathbf{L}_p = \sum_{\alpha} \dot{\gamma}^{(\alpha)}\, \mathbf{P}^{(\alpha)} \tag{2}$$

It should be noted that $\mathbf{s}^{(\alpha)}$ and $\mathbf{n}^{(\alpha)}$ are computed by means of the lattice rotations. In the kinetics of crystallographic deformations, plastic flow occurs once the resolved shear stress on each slip system $\tau^{(\alpha)} = \boldsymbol{\sigma} : \mathbf{P}^{(\alpha)}$ exceeds the slip resistance $\tau_c^{(\alpha)}$. To find the Cauchy stress tensor, the corotational rate of this tensor $\overset{\triangledown}{\boldsymbol{\sigma}}$ is related to the rate of elastic deformation $\mathbf{D}_e$ as

$$\overset{\triangledown}{\boldsymbol{\sigma}} = \mathbb{C}_e : \mathbf{D}_e \tag{3}$$

In Eq. (3), $\mathbf{D}_e$ is the elastic velocity gradient tensor and $\mathbb{C}_e$ stands for the constant elastic stiffness tensor [18].

A Taylor hardening law is employed in the current model. Due to the impediment of the dislocation motion by an increase in the forest dislocations, critical resolved shear stress (CRSS) keeps increasing with the increase of plastic deformation. Thus the work hardening law as Eq. (4) is applied in which τ_0 is the strain-independent lattice friction, μ is the shear modulus, b is the length of the Burgers vector, $\rho^{(\beta)}$ is the dislocations density of the slip system β and $Q^{(\alpha\beta)}$ is the interaction matrix that takes the geometrical relationship and position of the slip systems into account. This matrix determines how an increase of the dislocation density on slip system β leads to the strengthening of slip system α. The diagonal elements of Q represent the slip system's self-hardening, and the off-diagonal elements indicate the influence of other slip systems.

$$\tau_c^{(\alpha)} = \tau_0 + \mu b \sqrt{\sum_{\beta} Q^{(\alpha\beta)} \rho^{(\beta)}} \tag{4}$$

Three cases are assumed for an FCC-based polycrystalline material with 12 slip systems. In the first case, the diagonal elements of the Q matrix are 1.0, and the off-diagonal ones are equal to 1.4 [19] (Case 1). In the second case, all elements of the Q matrix are assumed to be 1.0, which means an isotropic state of self and the latent hardening of slip systems holds (Case 2). In the last case, all diagonal terms of the Q matrix are 1.0, and all off-diagonal elements are zero. It means that each slip system only hardens itself (Case 3). Although Case 3 is unrealistic, it is considered to study how the interaction of the slip systems contributes to hardening. The results section will further discuss the influence of various interaction matrices.

The evolution of dislocation densities on slip system α, which mainly depends on the shear rate on this slip system, is formulated on a phenomenological basis in terms of a linear ordinary differential equation as

$$\dot{\rho}^{(\alpha)} = \frac{\dot{\gamma}^{(\alpha)}}{\gamma^{\infty}} [\rho^{\infty} - \rho^{(\alpha)}] \tag{5}$$

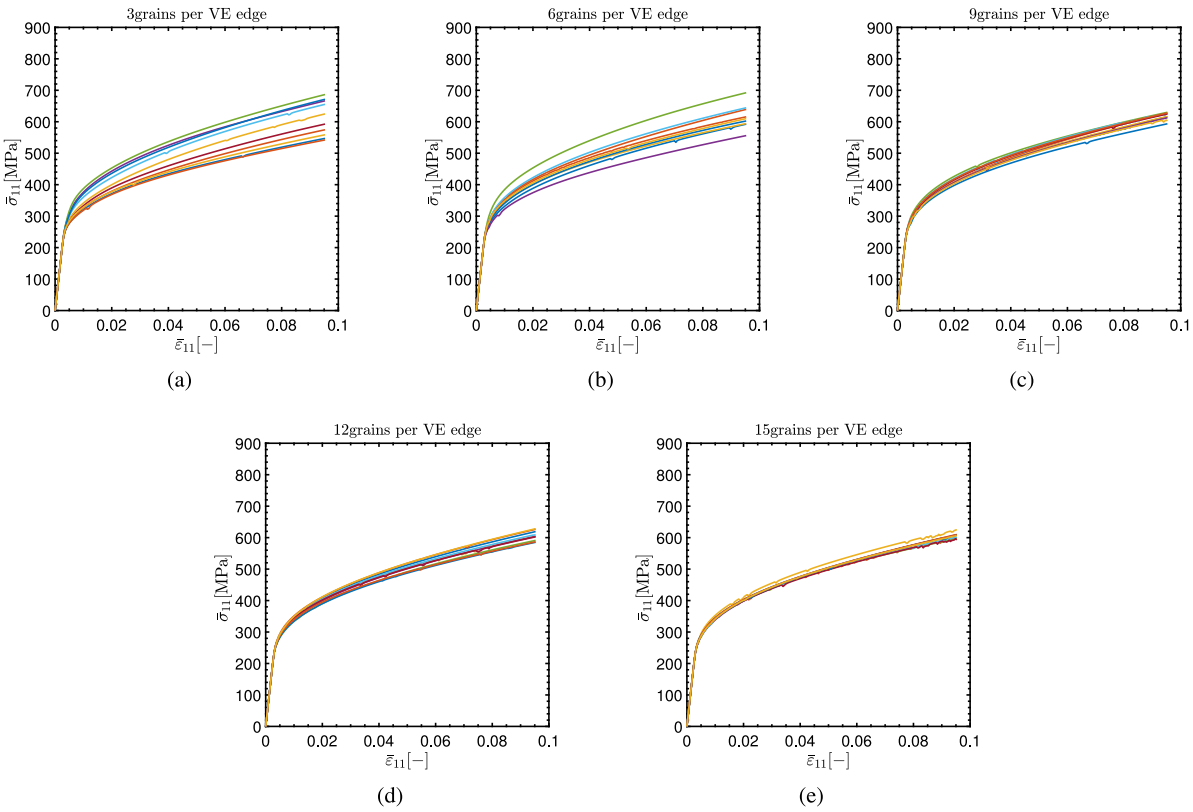

Fig. 2. Determination of the size of 2D RVE. Ten stochastic generations are used per number of grains per VE edge (3,6,9,12,15). Average true stress–true strain curves for all VEs are presented in the loading direction.

In Eq. (5), $\dot{\gamma}^{(\alpha)}$, $\rho^{(\alpha)}$ and $\dot{\rho}^{(\alpha)}$ are the rate of slip, the dislocation densities and their rate on slip system α, whereas γ^{∞} and ρ^{∞} indicate the saturated slip and dislocation densities, respectively. Eq. (5) denotes the balance between the generation of dislocations by the Frank-Read mechanism and dislocation annihilation. For the details of the implementation of the numerical solution to the stress update algorithm in this model, one can refer to [15].

3. Computational homogenization

Computational homogenization is a methodology to determine the constitutive behavior of a material considering microstructural aspects. This can be achieved through an RVE-based finite element analysis assuming periodic boundary conditions. In solving the nested boundary value problem (BVP) of the micro equilibrium equations under certain boundary conditions, microscopic stresses need to be translated into macroscopic stress. The proper selection of the RVE is a delicate task. Based on the definition, an RVE must be adequately large to be statistically representative of the material characteristics and sufficiently small to sample the microstructural heterogeneities [20]. For a specific microstructure, several RVEs with geometrically periodic boundaries might lead to valid predictions of the material response. Confinement of an RVE with a cuboidal shape might cause short edges on the exterior edges. Irregularly shaped but geometrically periodic RVEs [21–23] are generated using Voro++ software library [24]. Fig. 1 illustrates a schematic of an RVE with 125 grains. Various colors of the grains represent attributed grain orientations. Periodic boundary conditions are assigned on the volume elements using the procedure explained in [25]. When the CPFE simulations in 2D and 3D are performed, an approach presented in [26] is used to compute the macroscopic stress components.

4. Results and discussion

Crystal plasticity finite element simulations of 2D and 3D RVEs are performed with local and averaged plane strain assumptions, respectively. Statistically stored dislocations have been assumed as the mere source of strain hardening in this study and the impact of strain gradients resulting in microstructural size effects is neglected. In the finite element simulations, each grain is assigned with a random orientation to reproduce untextured polycrystalline material. The material parameters used in the crystal plasticity model are presented in Table 1. To compare the material response in 2D and 3D cases, the required minimal RVE size has to be determined. Thus various 2D and 3D volume elements are generated, increasing the number of grains per volume element edge. For each number of grains, multiple sets of volume elements with different combinations of grain orientations were generated to check whether the resulting macroscopic flow curves approach each other. Consequently, a narrow scatter band for all volume elements with a specific number of grains implies that the material response is independent of the statistical aspects related to the volume element; hence, the volume element is representative of the material characteristics at the macroscale. The procedure of the RVE size determination is displayed in Figs. 2 and 3. Based on Figs. 2 and 3, it is concluded that 225-grain volume elements (15 grains per VE edge) and 125-grain volume elements (5 grains per VE edge) are the appropriate RVE size in the 2D and 3D case, respectively. It is noticed that the plane strain condition is imposed by plane strain elements in the 2D case; the thickness strain and both out-of-plane shear strains are zero at all integration points. However, in 3D, the average thickness and out-of-plane shear strains are considered zero. The grains are allowed to strain individually in the thickness direction, but the average strain vanishes alongside the thickness.

To clarify the RVE size determination, another representation of the results is displayed in Fig. 4. In this figure, the average stress in

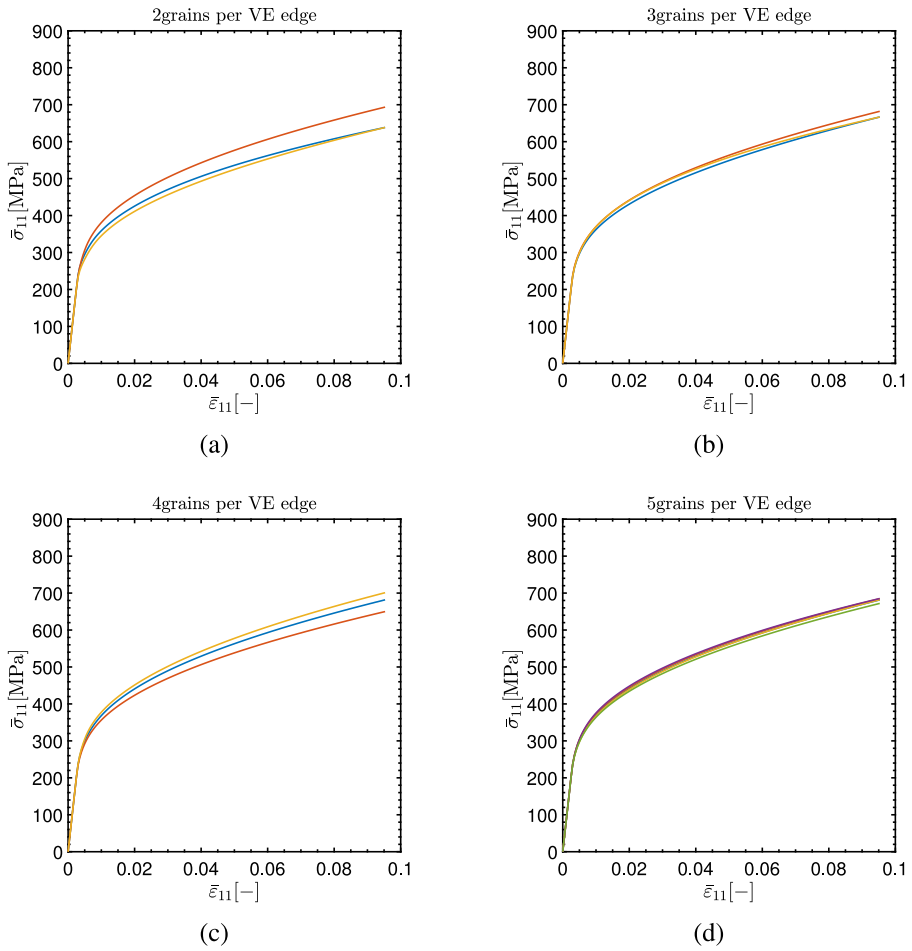

Fig. 3. Determination of the size of 3D RVE. Three stochastic generations are used per number of grains per VE edge (2 to 4) and five stochastic generations are used for 5 grains per VE edge. Average true stress–true strain curves for all VEs are displayed in the loading direction.

Table 1
Material parameters for Aluminum with FCC crystal structure used in CPFE simulations.

Property	Symbol	Magnitude
Young's modulus	E	72 GPa
Poisson's ratio	ν	0.33
Length of Burgers vector	b	2.86×10^{-7} mm
Initial dislocation density	ρ_0	10^5 mm^{-2}
Saturation dislocation density	ρ_∞	10^{11} mm^{-2}
Saturation shear strain	γ_∞	10
Initial critical resolved shear strength	τ_0	100 MPa
Slip interaction parameter, Case 1	$Q_{\alpha\beta}, \alpha \neq \beta$	1.4
Slip interaction parameter, Case 2	$Q_{\alpha\beta}, \alpha \neq \beta$	1.0
Slip interaction parameter, Case 3	$Q_{\alpha\beta}, \alpha \neq \beta$	0

the loading direction at the final engineering strain of 10% versus the number of grains per VE edge is shown in boxplots. In Fig. 4(a) for the 2D case, each box represents the values for ten datasets. The red line shows the median value among the data, and the lower and upper lines indicate the 25th and 75th percentiles, respectively. In the case of the existence of extreme data, it is indicated by means of a red '+' marker. It is clearly observed in Fig. 4(a) that the median value has converged for 14 and 15 grains per VE edge. In addition, the lower and upper bounds of the data are getting much closer for 14 and 15 grains than the rest of the numbers. In Fig. 4(b) for the 3D case, the median line settles at the same level for 4 and 5 grains per VE edge. The variation of the data, compared to the median value, is much less for 5 grains. The observation in Fig. 4, supports the RVE size selection elaborated earlier. In the RVE size determination procedure, Case 1 for the latent hardening of FCC crystallographic structure is applied, meaning that each slip system hardens itself by a factor of 1.0 and others with a factor of 1.4 [19]. The impact of different slip system interactions on material constitutive behavior will be addressed later.

Once the size of the RVE is decided, the macroscopic stress–strain curves obtained by 2D and 3D plane strain CPFE simulations are compared. The comparison is carried out regarding three different slip systems interactions, Cases 1,2 and 3, mentioned in Section 2. The reason for choosing three cases of latent hardening parameter is to check if this parameter affects the differences in 2D and 3D simulations, displayed later. These three cases are compared in Fig. 5. In Fig. 5(a), Case 1, the averaged flow curve of a 125-grain 3D RVE stands higher than a 225-grain 2D one. For Case 2, the 2D–3D discrepancy diminishes. In this case, the latent hardening coefficient has decreased from 1.4 in Case 1 to 1.0. In the last case, designated by Case 3, 2D and 3D flow curves are far closer to each other. Still, in this case, the material strain hardening has decreased compared to the other two cases. The high discrepancy captured in Cases 1 and 2 is caused by the extra slip occurring in the thickness direction of 3D RVEs. With high latent hardening, a small deformation in the plane strain direction can remarkably affect the loading direction. Full plane strain, in the 2D case, imposes more constraints than the average plane strain in the 3D case, and one would expect higher stress if all other conditions are the same, but this is not the dominating factor. The hypothesis is that the additional out-of-plane deformation, although statistically zero, gives extra hardening; therefore, the other conditions are not the same. This is further investigated, e.g., by comparing the average slip and CRSS on slip systems.

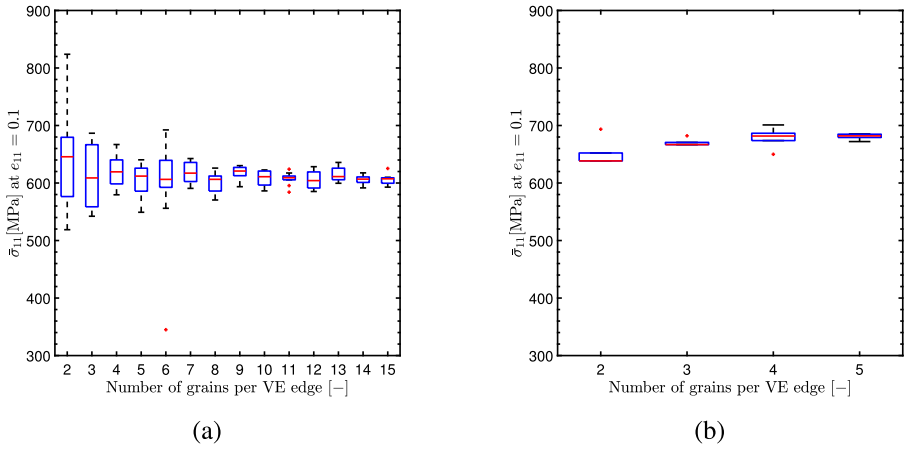

Fig. 4. The average stress in the loading direction at a final engineering strain of 10% versus the number of grains per VE edge. Each boxplot contains the data for 10 VEs in the 2D case (a) and for 3 VEs in the 3D case (b). It should be noted that the 3D case data for the grain number of 5 per VE edge includes five volume elements for certainty. The data is shown in terms of their median value. The bottom and top edges of the box display the 25th and 75th percentiles, respectively. Outliers are plotted individually using the red '+' marker symbol. (For interpretation of the references to color in this figure legend, the reader is referred to the web version of this article.)

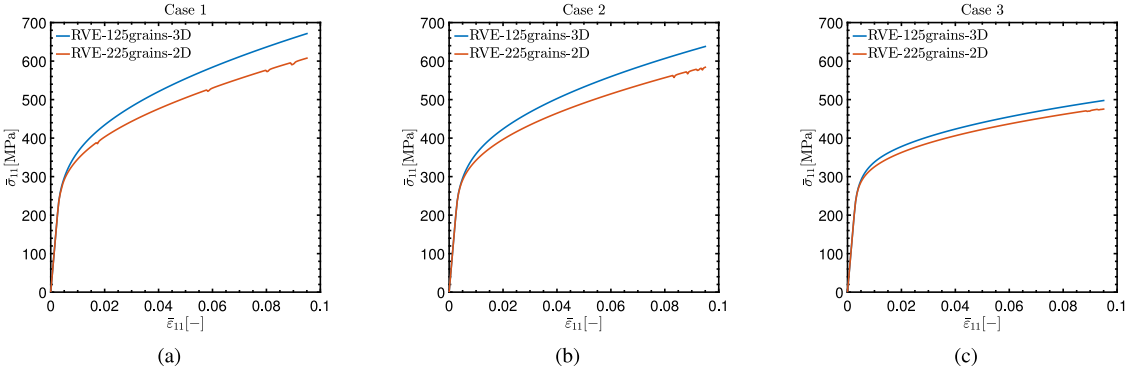

Fig. 5. Macroscopic flow curves in terms of the averaged true stress versus averaged true strain in the prescribed loading direction. (a) Case 1 with slip interaction parameter of 1.4, (b) Case 2 with isotropic latent hardening, (c) Case 3 with only self-hardening behavior.

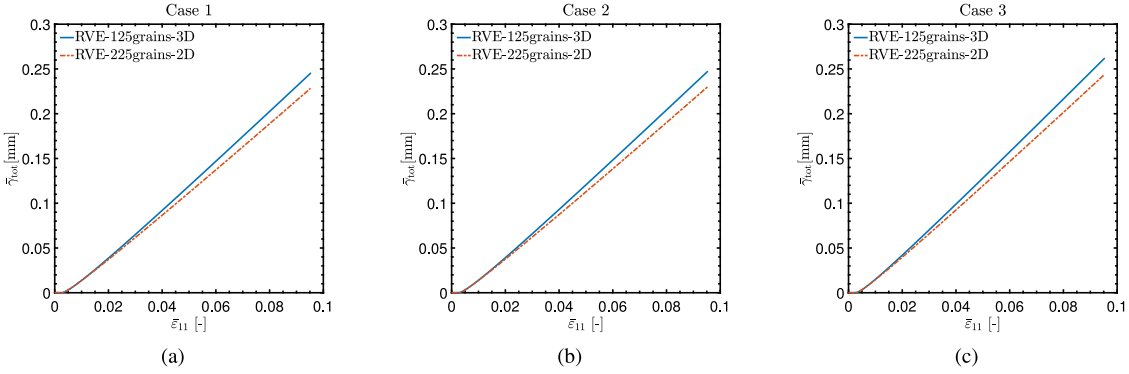

Fig. 6. Averaged total slip summed over all 12 FCC slip systems versus averaged true strain in the prescribed loading direction. (a) Case 1 with slip interaction parameter of 1.4, (b) Case 2 with isotropic latent hardening, (c) Case 3 with only self-hardening behavior.

Since all slip systems can contribute to almost all deformation directions, it is difficult to separate the effect of each slip system, and therefore, the total slip or average dislocation density and CRSS are presented. But it can be anticipated that the out-of-plane strain and shear, which is not in the main deformation direction, will have more effect on the stress in the main deformation direction if the latent hardening parameter is higher. This is indeed confirmed by Fig. 8.

To support our hypothesis, a comparison is made for the averaged sum of slip on all slip systems, dislocation densities and CRSS between 2D and 3D simulations. The averaged sum of slip on all slip systems with respect to the averaged strain in the loading direction is displayed in Fig. 6. According to this figure, for all three cases, the total slip in a 3D RVE is higher than the 2D one. Fig. 7 depicts the averaged total dislocation densities versus macroscopic strain in the loading direction. The dislocation densities in 3D RVEs are higher than in 2D ones. This observation is anticipated according to Eq. (5); which shows that an increase in the shear promotes the dislocation densities. Based upon Fig. 6 and Eq. (5), the dislocation densities in 3D RVEs must be higher than 2D RVEs. That is in accordance with the results obtained in Fig. 7. Figs. 6 and 7 show that the latent hardening parameter hardly

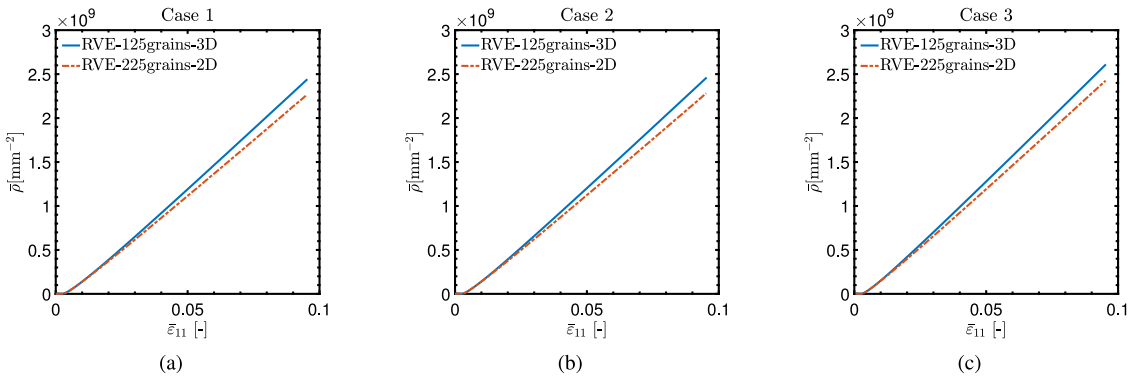

Fig. 7. Averaged total dislocation densities summed over all 12 FCC slip systems versus averaged true strain in the prescribed loading direction. (a) Case 1 with slip interaction parameter of 1.4, (b) Case 2 with isotropic latent hardening, (c) Case 3 with only self-hardening behavior.

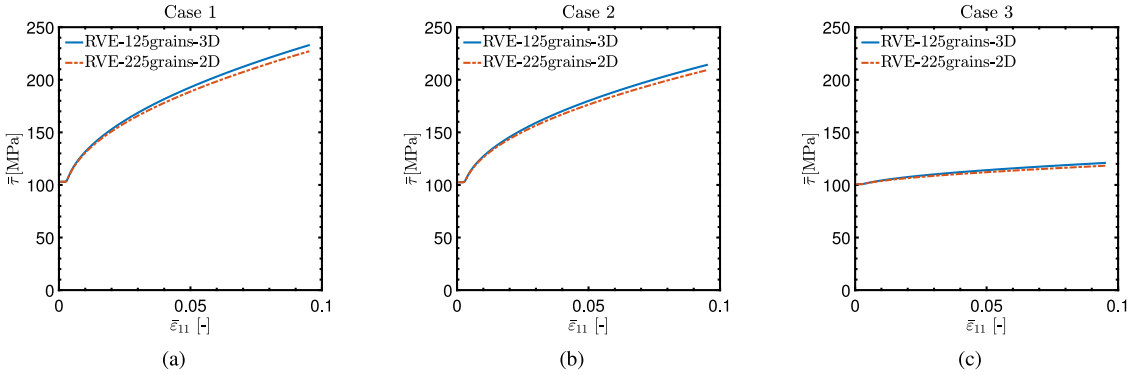

Fig. 8. Averaged CRSS versus averaged true strain in the prescribed loading direction. The 3D results are displayed in solid lines whereas 2D ones are plotted in dash lines (a) Case 1 with slip interaction parameter of 1.4, (b) Case 2 with isotropic latent hardening, (c) Case 3 with only self-hardening behavior.

influences the averaged total slip and dislocation densities. It is, to a large extent, kinematically determined.

The evolution of the averaged CRSS with averaged strain in the prescribed loading direction is compared for 2D and 3D RVEs in Fig. 8. In all three cases, there is a plateau in the initial stages of straining. This value shows the initial lattice friction. After a specific point, the slip systems are activated, and the material hardens. Hence, CRSS increases. Based upon Fig. 8, in Cases 1 and 2, the averaged CRSS in 3D consistently exceeds the 2D values. The averaged total slip and dislocation densities are higher in 3D simulations (Figs. 6 and 7); hence, the CRSS must be higher in 3D models.

The influence of the latent hardening parameter supports the conclusion that out-of-plane deformation influences the in-plane stresses via the hardening relation. It is only an indication since the slip systems contribute to many directions.

To recapitulate, the discrepancy of the macroscopic material response in 2D and 3D CPFE simulations is assumed to be caused by the extra slip in the thickness direction in 3D, which finally averages to zero (Fig. 9). These out-of-plane slip systems activities promote a heterogeneity as indicated later in Fig. 10. To support this assumption, considering three cases of latent hardening (Cases 1 to 3), further analysis is carried out on the averaged total slip summed over all 12 FCC slip systems, averaged total dislocation densities summed over all 12 FCC slip systems and averaged CRSS. It is deduced from the numerical outputs that the total amount of slip at a particular total strain is higher in 3D than in 2D. The numerical observations also indicate that the averaged total slip and averaged total dislocation densities are hardly influenced by the amount of latent hardening since the deformation is kinematically determined. However, the CRSS is influenced in Cases 1 to 3. It is clear that all slip systems can contribute to almost all deformation directions. However, the extra slip occurring in the thickness direction in 3D CPFE simulations in the first two

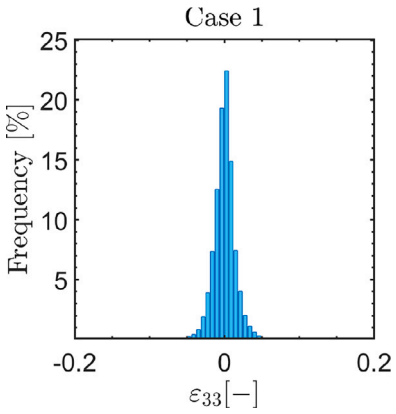

Fig. 9. Frequency of integration points in the 3D FEM model with a specific thickness strain at the final engineering strain of 10% for Case 1.

cases of latent hardening (Cases 1 and 2) is hardening the material in the loading direction significantly. These observations support the hypothesis that the higher hardening in 3D averaged plane strain crystal plasticity simulations, compared to 2D full plane strain simulations, originates from locally fluctuating out-of-plane deformations.

The distribution of the integration points in a 3D FEM model that experiences a certain engineering thickness strain at a prescribed loading strain for Case 1, 10% in the loading direction, is depicted in Fig. 9. This distribution is defined as the number of integration points within a thickness strain interval divided by the total number of integration points. Fig. 9 shows that the thickness strains sum up to zero in total. However, for a remarkable fraction of the integration points, the values

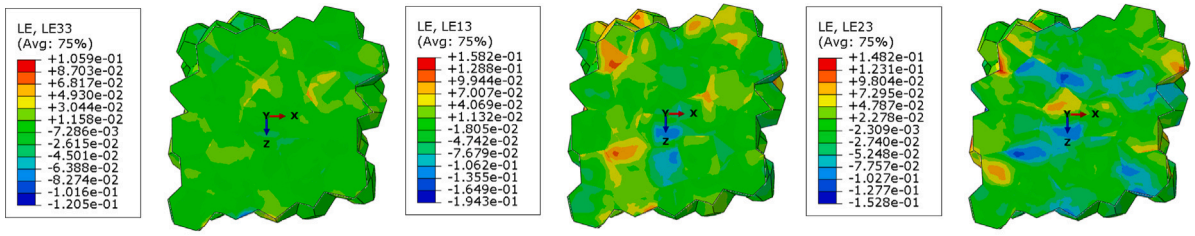

Fig. 10. Strains on a cut normal to y-axis of the 125-grain 3D RVE (Case 1) at prescribed engineering strain of 10% for (a) thickness strain (ε_{33}), (b) shear strain (ε_{13}), (c) shear strain (ε_{23}).

of the thickness strains are noticeable compared to the value of the strain in the loading direction. It is inferred that the thickness strain of individual grains is not negligible and contributes significantly to a higher strength of the material in 3D cases. This observation is in agreement with the results of Ramazani et al. [7].

The thickness strain and out-of-plane shear strains on a cut of a 125-grain 3D RVE, normal to y-axis, at a prescribed engineering strain of 10% for Case 1, are displayed in Fig. 10. This figure depicts the out-of-plane strains in 3D that cause higher hardening in 3D CPFE simulations. The shear strains in Fig. 10 show a strong inhomogeneity if presented in the principal loading directions.

5. Conclusion

This paper assesses the influence of the plane strain condition generally used to capture the material response in CPFE simulations. To achieve this goal, 2D and 3D CPFE simulations with irregularly shaped RVEs are carried out under the plane strain assumption. A macroscopic deformation gradient tensor is prescribed by which the displacements of periodic nodes are constrained in FEM simulations. This implementation assures periodic boundary conditions. A rate-independent finite strain crystal plasticity model is used as a user-defined material subroutine at each integration point.

The macroscopic flow curves of the 3D RVEs exceed the curves for 2D RVEs for all three cases of slip systems interaction. This behavior results from the extra deformation that occurs in the thickness direction in the 3D case. The high discrepancy of the flow curve for Case 1 highlights the necessity for 3D simulations. The averaged CRSS, averaged total slip, and total dislocation densities in 3D simulations all exceed the values for 2D simulations. Although the average thickness strain is zero in a 3D case, individual grains can still deform in this direction. These out-of-plane deformations result in a higher material strength in 3D simulations.

Declaration of competing interest

The authors declare that they have no known competing financial interests or personal relationships that could have appeared to influence the work reported in this paper.

Data availability

Data will be made available on request.

Acknowledgments

This research was carried out under project number T17019a in the framework of the Research Program of the Materials innovation institute (M2i) (www.m2i.nl) supported by the Dutch government and Tata Steel company. The authors thank Dr. Celal Soyarslan for sharing his vision, thoughts and information.

References

[1] I. Babuška, Homogenization and its application. Mathematical and computational problems, in: Numerical Solution of Partial Differential Equations–III, Elsevier, 1976, pp. 89–116.
[2] R. Hill, Elastic properties of reinforced solids: Some theoretical principles, J. Mech. Phys. Solids 11 (5) (1963) 357–372.
[3] F. Roters, P. Eisenlohr, T.R. Bieler, D. Raabe, Crystal Plasticity Finite Element Methods: In Materials Science and Engineering, John Wiley & Sons, 2011.
[4] J. Rossiter, A. Brahme, M. Simha, K. Inal, R. Mishra, A new crystal plasticity scheme for explicit time integration codes to simulate deformation in 3D microstructures: Effects of strain path, strain rate and thermal softening on localized deformation in the aluminum alloy 5754 during simple shear, Int. J. Plast. 26 (12) (2010) 1702–1725.
[5] R. Esmaeilpour, H. Kim, T. Park, F. Pourboghrat, Z. Xu, B. Mohammed, F. Abu-Farha, Calibration of Barlat Yld2004-18P yield function using CPFEM and 3D RVE for the simulation of single point incremental forming (SPIF) of 7075-o aluminum sheet, Int. J. Mech. Sci. 145 (2018) 24–41.
[6] A. Vuppala, X. Wei, S. Hojda, M. Teller, G. Hirt, Investigation of texture evolution during rolling simulation of non-oriented Si based electrical steels with 2D and 3D RVE, in: Proceedings of the 6th European Conference on Computational Mechanics, Glasgow, UK, 2018, pp. 11–15.
[7] A. Ramazani, K. Mukherjee, H. Quade, U. Prahl, W. Bleck, Correlation between 2D and 3D flow curve modelling of DP steels using a microstructure-based RVE approach, Mater. Sci. Eng. A 560 (2013) 129–139.
[8] C. Thomser, Modelling of the Mechanical Properties of Dual Phase Steels Based on Microstructure, (Ph. D. thesis), RWTH-Aachen, Germany, 2009.
[9] F. Qayyum, A.A. Chaudhry, S. Guk, M. Schmidtchen, R. Kawalla, U. Prahl, Effect of 3D representative volume element (RVE) thickness on stress and strain partitioning in crystal plasticity simulations of multi-phase materials, Crystals 10 (10) (2020) 944.
[10] M. Knezevic, B. Drach, M. Ardeljan, I.J. Beyerlein, Three dimensional predictions of grain scale plasticity and grain boundaries using crystal plasticity finite element models, Comput. Methods Appl. Mech. Engrg. 277 (2014) 239–259.
[11] A. Acharya, A model of crystal plasticity based on the theory of continuously distributed dislocations, J. Mech. Phys. Solids 49 (4) (2001) 761–784.
[12] S. Forest, R. Sievert, E.C. Aifantis, Strain gradient crystal plasticity: Thermomechanical formulations and applications, J. Mech. Behav. Mater. 13 (3–4) (2002) 219–232.
[13] D.J. Bammann, A model of crystal plasticity containing a natural length scale, Mater. Sci. Eng. A 309 (2001) 406–410.
[14] J.R. Mayeur, D.L. McDowell, A three-dimensional crystal plasticity model for duplex Ti–6Al–4V, Int. J. Plast. 23 (9) (2007) 1457–1485.
[15] E.E. Asik, E.S. Perdahcioglu, A.H. van den Boogaard, An RVE-based study of the effect of martensite banding on damage evolution in dual phase steels, Materials 13 (7) (2020).
[16] R.J. Asaro, Crystal plasticity, J. Appl. Mech. 50 (1983) 921–934.
[17] J.D. Clayton, Nonlinear Mechanics of Crystals, Vol. 177, Springer Science & Business Media, 2010.
[18] M.H. Sadd, Elasticity: Theory, Applications, and Numerics, Academic Press, 2009.
[19] C. Gérard, G. Cailletaud, B. Bacroix, Modeling of latent hardening produced by complex loading paths in FCC alloys, Int. J. Plast. 42 (2013) 194–212.
[20] P. Gumbsch, R. Pippan, Multiscale Modelling of Plasticity and Fracture By Means of Dislocation Mechanics, Vol. 522, Springer Science & Business Media, 2011.
[21] M. Nygårds, P. Gudmundson, Three-dimensional periodic voronoi grain models and micromechanical FE-simulations of a two-phase steel, Comput. Mater. Sci. 24 (4) (2002) 513–519.
[22] N. Kowalski, L. Delannay, P. Yan, J.-F. Remacle, Finite element modeling of periodic polycrystalline aggregates with intergranular cracks, Int. J. Solids Struct. 90 (2016) 60–68.

[23] A. Cruzado, J. Llorca, J.S. Escudero, Computational micromechanics modeling of polycrystalline superalloys: Application to inconel 718, in: Integrated Computational Materials Engineering, ICME, Springer, 2020, pp. 127–163.
[24] C.H. Rycroft, A three-dimensional Voronoi cell library in C++, Technical Report LBNL-1432E, Lawrence Berkeley National Laboratory, 2009.
[25] C. Soyarslan, S. Bargmann, M. Pradas, J. Weissmüller, 3D stochastic bicontinuous microstructures: Generation, topology and elasticity, Acta Mater. 149 (2018) 326–340.
[26] V. Kouznetsova, W. Brekelmans, F. Baaijens, An approach to micro-macro modeling of heterogeneous materials, Comput. Mech. 27 (1) (2001) 37–48.